Polymer Journal (2023) 55:405–415
https://doi.org/10.1038/s41428-022-00706-z

ORIGINAL ARTICLE

Synthesis and solar cell applications of semiconducting polymers based on vinylene-bridged 5-alkoxy-6-fluorobenzo[*c*][1,2,5] thiadiazole (FOBTzE)

Hiroki Mori[1] · Yuya Asanuma[2] · Ryuchi Hosogi[2] · Yasushi Nishihara[1]

Received: 8 July 2022 / Revised: 8 August 2022 / Accepted: 9 August 2022 / Published online: 20 September 2022

Abstract

To improve the strong aggregation behavior and molecular orientation of the previously reported polymer **PFE4T** with vinylene-bridged 5,6-difluorobenzo[*c*][1,2,5]thiadiazole (FBTzE), we designed and synthesized a vinylene-bridged 5-alkoxy-6-fluorobenzo[*c*][1,2,5]thiadiazole (FOBTzE) moiety as a novel electron acceptor unit and its copolymer **PFOE4T**. By installing a strong electron-donating alkoxy group into the FBTzE framework instead of an electron-withdrawing fluorine atom, the highest occupied molecular orbital (HOMO) energy level of the resulting polymer **PFOE4T** was found to be ca. 0.1 eV higher than that of the previously reported polymer **PFE4T** but comparable to that of typical difluorobenzothiadiazole-based polymers. On the other hand, the introduction of alkoxy side chains reduced the strong aggregation tendency and changed the molecular orientation of the polymers from edge-on to bimodal orientation, providing a uniform polymer blended film with $PC_{61}BM$ and enhancing carrier transport. These results indicate that the fabricated **PFOE4T**/$PC_{61}BM$-based solar cells exhibited a power conversion efficiency of 4.52% with a high fill factor (FF) of 0.68. However, because **PFOE4T** still has strong aggregation and low solubility, the **PFOE4T**/$PC_{61}BM$ blended film formed a large phase separation, resulting in limited short-circuit current density (J_{sc}) and PCE.

Introduction

π-Conjugated polymers with donor–acceptor (D–A)-type architectures are important functional materials for organic photovoltaics (OPVs) because of their high light-harvesting ability in the visible and near-infrared (NIR) regions, strong intermolecular interactions due to Coulomb interactions, and easy tuning of highest occupied molecular orbital (HOMO)–lowest unoccupied molecular orbital (LUMO) energy levels, enabling high photocurrent conversion and carrier transport in OPVs [1–7]. Over the past two decades, a wide variety of developments have been made on D–A π-conjugated polymers with high power conversion efficiency (PCE) [1–7].

To design high-performance π-conjugated polymers for OPVs, tuning the electronic structure and polymer geometry is highly important to maximize PCE. For instance, since the open-circuit voltage (V_{oc}) is strongly related to the energy difference between the HOMO energy level of the p-type polymer and the LUMO energy level of the n-type material, deeping the HOMO energy level of the p-type polymer can increase the V_{oc} of the fabricated solar cells [8, 9]. Furthermore, small HOMO–HOMO or LUMO–LUMO offsets between the p-type and n-type materials in OPVs have been found to reduce the energy loss in OPV devices, resulting in higher V_{oc} [7, 10, 11]. The optical bandgap (E_g) of D–A type π-conjugated polymers is directly related to their light-harvesting ability, and the wide bandgap p-type polymers can achieve complementary absorption with the commonly used low-bandgap nonfullerene acceptors

Supplementary information The online version contains supplementary material available at https://doi.org/10.1038/s41428-022-00706-z.

✉ Hiroki Mori
h-mor@okayama-u.ac.jp

✉ Yasushi Nishihara
ynishiha@okayama-u.ac.jp

[1] Research Institute for Interdisciplinary Science, Okayama University, 3-1-1 Tsushimanaka, Kita-ku, Okayama 700-8530, Japan

[2] Graduate School of Natural Science and Technology, Okayama University, 3-1-1 Tsushimanaka, Kita-ku, Okayama 700-8530, Japan

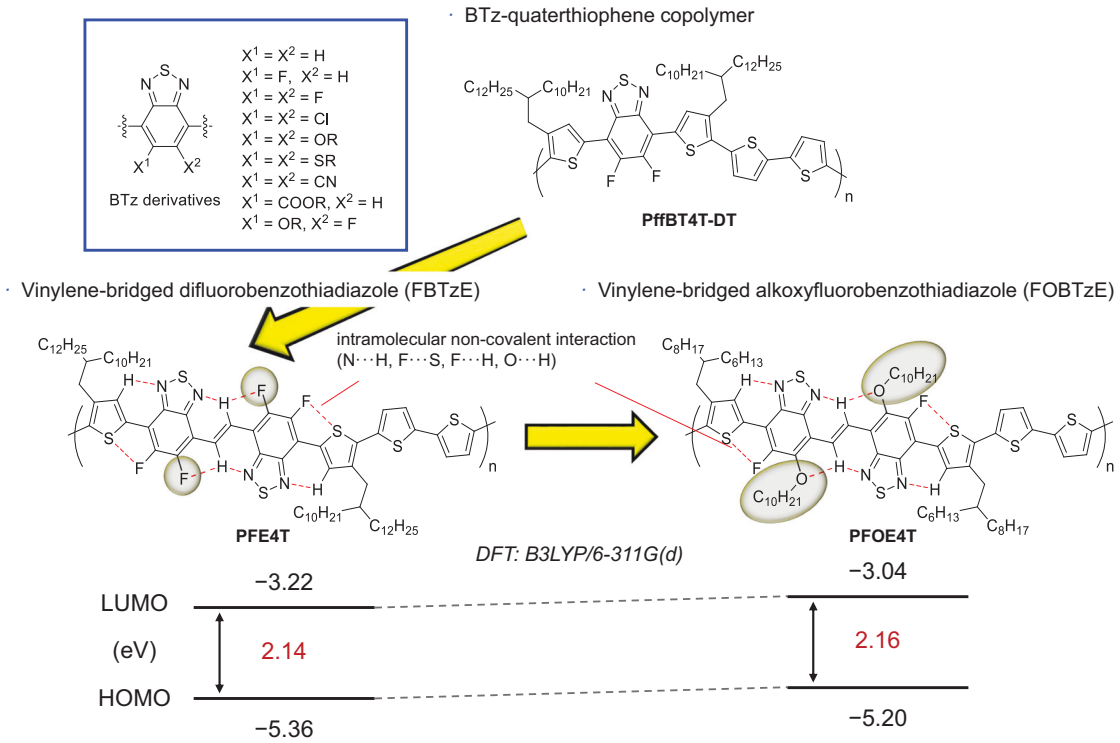

Fig. 1 Chemical structures of the BTz derivatives, **PffBT4T-DT**, **PFE4T**, and **PFOE4T**, and HOMO and LUMO energy levels of the model compounds calculated by DFT calculations (B3LYP/6-311 G(d))

(NFA, n-type component) to efficiently generate photocurrent, resulting in a high short-circuit current density (J_{sc}) [12, 13]. On the other hand, the construction of desirable structural motifs, such as high crystallinity, face-on orientation, and nanoscale morphology, is believed to lead to high carrier mobility and efficient charge separation, which are crucial for J_{sc} and the fill factor (FF) [14–17]. The desirable thin-film structure could be obtained by optimizing the side chain and backbone geometry [14, 15, 17, 18]. Therefore, the optimal combination of D and A units in D–A-type π-conjugated polymers is highly important to achieve high PCE in OPVs.

5,6-Functionalized benzo[*c*][1,2,5]thiadiazoles (BTz, Fig. 1) are among the most finely tunable electron acceptor units in high-performance D–A-type π-conjugated polymers in OPVs in terms of their molecular structure [1–4, 6, 19, 20]. Indeed, various functional groups, such as electron-donating alkoxy [21–24] and thioalkyl [25] groups, electron-withdrawing halogen atoms (fluorine [18, 26–30] and chlorine [31–33]), alkoxycarbonyl [34] and cyano [35, 36] groups, have been employed in the BTz framework to fine-tune the electronic properties and thin-film structure of D–A-type π-conjugated polymers. For instance, the introduction of an electron-withdrawing fluorine atom into the BTz framework has been shown to result in a downshift of the HOMO and LUMO energy levels and an increase in coplanarity of the resulting D–A polymers due to intramolecular noncovalent interactions, leading to higher V_{oc} and the construction of an ordered packing structure [18, 26–30]. On the other hand, the introduction of a strong electron-donating alkoxy group into the BTz unit can reduce the electron affinity of the BTz unit, resulting in a wider E_g [21–24]. The flexible alkoxy chains on the BTz units also enhance the solubility of the polymer without interfering with the ordered packing structure of the polymer backbone and can easily control the internal morphology [37]. Therefore, the development of acceptor units containing thiadiazoles, which can be readily functionalized, is an efficient way to fine-tune the HOMO and LUMO energy levels of D–A-type π-conjugated polymers.

Previously, we reported vinylene-bridged difluorobenzothiadiazole (FBTzE) as a new electron acceptor unit and its copolymers **PFBTzEAr-R** with alkylated oligothiophenes as donor units [38–40]. Interestingly, the FBTzE-quaterthiophene copolymer (**PFE4T**, Fig. 1) has lower-lying HOMO and LUMO energy levels than the typical difluorobenzothiadiazole (DFBT)-based polymer **PffBT4T-DT** due to the presence of two DFBT units in the FBTzE core [38], indicating that it may be beneficial for developing high-performance p-type polymers and n-type semiconductors in OPVs. Furthermore, the incorporation of a π-extended, highly planar FBTzE core through various intramolecular noncovalent interactions can promote effective π-orbital overlap in the resulting polymer **PFE4T**, leading to a highly ordered packing structure with stronger intermolecular interactions than **PffBT4T-DT** and a shorter π-stacking distance of 3.5 Å

[38, 39]. As a result, **PFE4T** exhibited a high hole mobility of up to 0.08 $cm^2 V^{-1} s^{-1}$ in organic field-effect transistors (OFETs) [39]. However, a uniform thin film of the **PFE4T**/$PC_{61}BM$ blend could not be obtained because of the excessively strong aggregation tendency, resulting in severe current leakage and thus the inability to achieve photovoltaic conversions [38]. To improve solubility without changing the coplanarity of the polymer, we designed vinylene-bridged 5-alkoxy-6-fluorobenzo[*c*][1,2,5]thiadiazoles (FOBTzE) and its copolymer **PFOE4T** (Fig. 1). 5-Alkoxy-6-fluorobenzo[*c*][1,2,5]thiadiazoles are also well-known acceptor units for high-performance D-A type π-conjugated polymers [37, 41–44]. Although the introduction of an electron-donating alkoxy group instead of the electron-withdrawing fluorine atom increases the HOMO and LUMO energy levels as well as slightly widens E_g (Figs. 1 and S1), the HOMO and LUMO energy levels are comparable to those of the typical difluorobenzothiadiazole-based polymer **PffBT4T-DT** [38]. In addition, the introduction of alkoxy side chains into the FBTzE framework can increase solubility and side-chain attachment density, enabling easy control of the morphology and molecular orientation of the resulting polymers [14, 18, 41–44]. Moreover, the presence of an alkoxy group in the core of FOBTzE enabled intramolecular noncovalent interactions between the oxygen atom of the alkoxy group and the hydrogen atom of the neighboring vinylene moiety, maintaining a high degree of coplanarity and an ordered packing structure [21–24, 41–45]. Herein, we report the synthesis, characterization, and solar cell applications of the FOBTzE-based polymer **PFOE4T** in combination with $PC_{61}BM$. In addition, the effects of the FOBTzE core on its electronic properties, thin-film structure, and photovoltaic properties will also be discussed.

Experimental section

General

All reactions were carried out by standard Schlenk techniques under an Ar atmosphere. Glassware was dried in an oven (130 °C) and heated under reduced pressure prior to use. Dehydrated tetrahydrofuran (THF), methanol (MeOH), dimethyl sulfoxide (DMSO), and toluene were purchased from Kanto Chemicals Co., Ltd. For thin layer chromatography (TLC) analysis, Merck precoated TLC plates (silica gel 60 GF_{254}, 0.25 mm) were used. Silica gel column chromatography was carried out using silica gel 60 N (spherical, neutral, 40–100 μm) from Kanto Chemicals Co., Ltd. ^1H, $^{13}C\{^1H\}$, and $^{19}F\{^1H\}$ NMR spectra were recorded on Varian 400-MR (400 MHz), Varian INOVA-600 (600 MHz), and JEOL JNMECZ600R (600 MHz) spectrometers. Infrared spectra were recorded on a Shimadzu IRPrestige-21 spectrophotometer. Elemental analysis was carried out on a Perkin-Elmer 2400 CHN elemental analyzer at Okayama University. Polymerization was performed in a Biotage initiator$^+$ microwave reactor. The molecular weights of the polymers were determined by gel permeation chromatography (GPC) at 140 °C using TOSOH HLC-8321GPC/HT and TSKgel GMH_{HR}-H HT with polystyrene standard and *o*-dichlorobenzene (*o*-DCB) as eluent.

Synthetic procedures

(*E*)-1,2-Bis(5,6-difluorobenzo[*c*][1,2,5]thiadiazol-4-yl)ethene (FBTzE) (**1**) (Scheme S1) [38], 2-bromo-3-(2-hexyldecyl) thiophene (**3**) [38], 3-cyclohexyl-2,2-dimethylpropanoic acid (**4**) [46], and 5,5'-bis(trimethylstannyl)-2,2'-bithiophene (**6**) [47] were synthesized according to reported procedures. Other chemicals were used without further purification unless otherwise indicated.

Synthesis of (*E*)-1,2-bis(5-decyloxy-6-fluorobenzo[*c*][1,2,5] thiadiazol-4-yl)ethene (2)

Sodium hydride (NaH, 60%, dispersion in a paraffin solution) (70.6 mg, 1.76 mmol) was added to a 20 mL Schlenk tube to a solution of 1-decanol (178 mg, 1.13 mmol) in anhydrous THF (9.3 mL). After the reaction mixture was stirred at 0 °C for 1 h, the mixture was warmed to room temperature, and (*E*)-1,2-bis(5,6-difluorobenzo[*c*][1,2,5] thiadiazol-4-yl)ethene (FBTzE, **1**) (167 mg, 0.45 mmol) was added. After the reaction mixture was refluxed for 12 h, the mixture was cooled to room temperature, and 20 mL of water was added. The crude mixture was extracted with dichloromethane (20 mL × 3), washed with brine, and dried over $MgSO_4$. After removal of the solvent under reduced pressure, the obtained solid was purified by silica gel column chromatography using hexane–dichloromethane (1:2) as the eluent ($R_f = 0.66$) to afford **2** (273 mg, 0.42 mmol) in 94% yield as a yellow solid; mp 106–108 °C. FT-IR (KBr, cm^{-1}): 3069 (m), 2951 (m), 2918 (s), 2847 (s), 1449 (s), 1310 (s), 1190 (m), 1015 (m), 868 (m), 687 (m). ^1H NMR (600 MHz, $CDCl_3$, rt): δ 0.87 (t, $J = 7.2$ Hz, 6H), 1.23-1.31 (m, 20H), 1.40 (quint, $J = 7.8$ Hz, 4H), 1.59 (quint, $J = 7.8$ Hz, 4H), 1.98 (quint, $J = 7.8$ Hz, 4H), 4.24 (t, $J = 6.6$ Hz, 4H), 7.60 (d, $J = 10.2$ Hz, 2H), δ 9.10 (s, 2H). $^{13}C\{^1H\}$ NMR (151 MHz, $CDCl_3$, rt): δ 14.3, 22.8, 26.1, 29.5, 29.7, 29.7_5, 29.7_8, 30.5, 32.0, 76.0, 104.6 (d, $J = 22$ Hz), 122.9 (d, $J = 4$ Hz), 127.1 (d, $J = 4$ Hz), 148.8 (d, $J = 17$ Hz), 151.0, 151.8 (d, $J = 14$ Hz), 159.4 (d, $J = 257$ Hz). $^{19}F\{^1H\}$ NMR (376 MHz, $CDCl_3$, rt): δ − 121.19. Anal. Calcd for $C_{34}H_{46}F_2N_4O_2S_2$: C, 63.33; H, 7.19; N, 8.69%. Found: C, 63.20; H, 7.12; N, 8.54%.

Synthesis of (*E*)-1,2-Bis{7-[5-bromo-4-(2-hexyldecyl) thiophen-2-yl]-5-decyloxy-6-fluorobenzo[*c*][1,2,5] thiadiazol-4-yl}ethene (5)

In a 20 mL Schlenk tube, to a solution of **2** (32.3 mg, 0.05 mmol), 2-bromo-3-(hexyldecyl)thiophene (**3**) (77.5 mg, 0.2 mmol), silver carbonate(I) (Ag_2CO_3) (110 mg, 0.4 mmol), and 3-cyclohexyl-2,2-dimethylpropanoic acid (**4**) (46 mg, 0.25 mmol) in anhydrous DMSO (0.5 mL) was added palladium(II) trifluoroacetate ($Pd(tfa)_2$) (3.3 mg, 0.01 mmol). The reaction mixture was heated to 140 °C for 24 h. The mixture was cooled to room temperature, and 5 mL of water was added. The crude mixture was extracted with dichloromethane (10 mL × 3), washed with 1 M hydrochloric acid and brine, and dried over $MgSO_4$. After removal of the solvent under reduced pressure, the obtained solid was purified by silica gel column chromatography using hexane–dichloromethane (2:1) as the eluent ($R_f = 0.92$) to afford **5** (14.2 mg, 0.01 mmol) in 20% yield as a red solid; mp 42–43 °C. FT-IR (KBr, cm^{-1}): 2953 (s), 2922 (s), 2853 (s), 1466 (m), 1437 (m), 1315 (m), 1165 (w), 1051 (w), 993 (w), 895 (w), 851 (w), 775 (w), 721 (w). ^1H NMR (600 MHz, $CDCl_3$, rt): δ 0.85-0.91 (m, 18H), 1.20-1.40 (m, 68H), 1.44 (quint, $J = 7.2$ Hz, 4H), 1.63 (quint, $J = 7.8$ Hz, 4H), 1.74 (m, 2H), 2.02 (quint, $J = 7.2$ Hz, 4H), 2.55 (d, $J = 6.6$ Hz, 4H), 4.22 (t, $J = 6.6$ Hz, 4H), 7.89 (s, 2H), 8.89 (s, 2H). $^{13}C\{^1H\}$ NMR (151 MHz, $CDCl_3$, rt): δ 14.3, 22.8_5, 22.8_7, 26.2, 26.6_5, 26.6_9, 29.5, 29.8_2, 29.8_5, 29.8_6, 29.8_9, 30.2, 30.7, 32.0, 32.1, 33.4_7, 33.5_4, 34.2, 38.7, 76.1, 111.6 (d, $J = 14$ Hz), 114.5 (d, $J = 10$ Hz), 121.1, 126.3, 132.0 (d, $J = 18$ Hz), 132.1, 141.6, 149.2 (d, $J = 19$ Hz), 149.7 (d, $J = 10$ Hz), 150.5, 154.9 (d, $J = 259$ Hz). $^{19}F\{^1H\}$ NMR (376 MHz, $CDCl_3$, rt): $\delta - 121.23$. Anal. Calcd for $C_{74}H_{112}Br_2F_2N_4O_2S_4$: C, 62.78; H, 7.97; N, 3.96%. Found: C, 62.76; H, 8.0; N, 3.75%.

Synthesis of polymer PFOE4T

Monomers **5** (70.8 mg, 0.05 mmol) and 5,5'-bis(trimethylstannyl)-2,2'-bithiophene (**6**) (24.6 mg, 0.05 mmol), tetrakis(triphenylphosphine)palladium(0) ($Pd(PPh_3)_4$, 1.2 mg, 1 μmol), copper iodide(I) (CuI, 1.0 mg, 5 μmol) and toluene (2.5 mL) were added to the reaction vessel, which was sealed and refilled with argon. The reaction mixture was heated in a microwave reactor at 140 °C for 30 min. After being cooled to room temperature, the reaction mixture was poured into 100 mL of methanol containing 5 mL of concentrated hydrochloric acid and stirred for 3 h. The precipitate was then subjected to sequential Soxhlet extraction with methanol, hexane, and chloroform to remove the low molecular-weight fraction. The residue was extracted with chlorobenzene, and the concentrated solution was poured into 25 mL of methanol. The precipitate formed was collected by filtration and dried in vacuo to afford the target polymer **PFOE4T** (62.6 mg, 88%) as a metallic purple solid; mp > 300 °C. ^1H NMR (600 MHz, *o*-dichlorobenzene-d_4, 100 °C): δ 0.80-0.90 (m, 18H), 1.20–1.60 (m, 72H), 1.71 (quint, $J = 6.9$ Hz, 4H), 2.01 (m, 2H), 2.15 (quint, $J = 6.8$ Hz, 4H), 2.99 (d, $J = 6.0$ Hz, 4H), 4.40 (brs, 4H), 7.24 (s, 4H), 8.40 (s, 2H), 9.23 (s, 2H). GPC (*o*-DCB, 140 °C): $M_n = 54.3$ kDa, $M_w = 110.8$ kDa, PDI = 2.04. Anal. Calcd for $C_{82}H_{118}F_2N_4O_2S_6$: C, 69.25; H, 8.36; N, 3.94%. Found: C, 69.27; H, 8.34; N, 3.70%.

Instrumentation and theoretical calculation

UV–vis absorption spectra were measured using a Shimadzu UV-2450 UV–vis spectrometer. Cyclic voltammograms (CVs) were recorded in acetonitrile containing tetrabutylammonium hexafluorophosphate ($TBAPF_6$, 0.1 M) as the supporting electrolyte at a scan rate of 100 mV/s on a CHI-600B Electrochemical Analyzer. Pt electrode (surface area: A = 0.071 cm^2, BAS), Ag/Ag^+ (Ag wire in 0.01 M $AgNO_3$/0.1 M $TBAPF_6/CH_3CN$) and Pt wire electrodes were used as the working, reference, and counter electrodes, respectively. Polymer films were prepared by drop casting on the working electrode from their chloroform solutions. All potentials were calibrated using a standard ferrocene/ferrocenium redox couple (Fc/Fc^+: $E^{1/2} = +0.03$ V for CH_3CN measured under identical conditions). Differential scanning calorimetry (DSC) was conducted at a rate of 10 °C/min from 25 °C to 250 °C for both heating and cooling steps under a nitrogen flow using a TA7000 (Hitachi High-Tech Corp., Japan). Dynamic force-mode atomic force microscopy (AFM) was carried out using an SPA 400-DFM (SII Nano Technologies). Grazing incidence wide-angle X-ray scattering (GIWAXS) analysis was carried out at SPring-8 on beamlines BL13XU and BL46XU. GIWAXS patterns were recorded with a 2D image detector (Pilatus 300 K) after fixed angle irradiation on the order of 0.12° through a Huber diffractometer with X-ray energy of 12.39 keV ($\lambda = 1$ Å). Polymer films and blended films with $PC_{61}BM$ were fabricated by spin-coating on ZnO-treated ITO substrates. Geometry optimization and normal-mode calculations were performed at the B3LYP/6-311 G(d) or M06-2X/6-311 G(d) level using the Gaussian 09 Revision D.01 program package [48].

Fabrication of inverted bulk-heterojunction solar cells

Inverted bulk-heterojunction solar cells were fabricated as follows. The ZnO precursor solution was prepared by the hydrolysis of $Zn(OAc)_2$ [49]. ITO substrates (ITO, Geomatec Co. Ltd., thickness = 150 nm, sheet resistance < 12 Ω sq^{-1}, transmittance ($\lambda = 550$ nm) ≥85%) were successively cleaned using ultrasonication in neutral detergent, deionized

water, acetone, and isopropanol at room temperature and in hot isopropanol for 10 min. The ITO substrates were then treated with UV-ozone for 20 min. The precleaned ITO substrates were spin-coated with 0.4 M ZnO precursor solution at 4000 rpm for 30 sec and immediately baked at 200 °C for 1 h in air. After gradual cooling to room temperature, the substrates were rinsed with acetone and isopropanol at room temperature, followed by a 5-min wash in hot isopropanol. The substrates were dried and immediately transferred to a nitrogen-filled glove box. An active layer with $PC_{61}BM$ was deposited by spin-coating at 600 rpm for 30 sec from a solution containing the polymer sample (4.0 mg/mL for **PFOE4T**) and each amount of $PC_{61}BM$ in anhydrous chlorobenzene (CB). The solution was held at 100 °C for 30 min and then spin-coated onto the substrate at room temperature. The p/n ratio is the weight ratio of the polymer to $PC_{61}BM$. Diphenyl ether (DPE, 1.0 vol%) was used as the solvent additive. MoO_3 (6 nm) as the anode interlayer and Ag (50 nm) layers were deposited under high vacuum (~5×10^{-5} Pa) through a shadow mask. The active area of all devices was 0.16 cm^2.

The characteristics of the solar cell devices were measured through a 4 × 4 mm photomask using a Keithley 2401 semiconductor analyzer with a Xe lamp (Bunkokeiki OTENTO-SAN III type G2) as the light source at room temperature under a nitrogen atmosphere and AM 1.5 G simulated solar irradiation at 100 $mWcm^{-2}$. Light intensity was determined with a calibrated standard silicon solar cell (Bunkokeiki, BS-520BK).

Fabrication and characterization of hole-only and electron-only devices

Hole-only devices were fabricated as follows. ITO substrates were cleaned in the same manner as described above. The precleaned ITO substrates were spin-coated with poly(3,4-ethylene-dioxythiophene):poly(styrene sulfonate) (PEDOT:PSS) (Clevios P VP AI 4083) at 5000 rpm for 30 sec through a 0.45 μm PVDF syringe filter. After drying at 150 °C in air for 15 min, the substrate was immediately transferred to a nitrogen-filled glove box. The active layer with $PC_{61}BM$ was deposited in the same manner as above (concentration: 6.0 mg/mL for **PFOE4T** with the same amount of $PC_{61}BM$). The thickness of the active layer was ca. 240 nm. After the active layer was dried under reduced pressure, MoO_3 (6 nm) and Ag (100 nm) were deposited in an area of 0.16 cm^2 through a shadow mask under high vacuum (~5×10^{-5} Pa). Electron-only devices were fabricated as follows. The ITO substrates were cleaned, and the ZnO layer was prepared in the same manner as described above. The **PFOE4T**/$PC_{61}BM$ active layer was deposited using the same method as above (concentration: 6.0 mg/mL). The thickness of the active layer was ca. 200 nm. After the active layer was dried under reduced pressure, an Ag (100 nm) electrode was deposited over a device area of 0.16 cm^2 through a shadow mask under high vacuum (~5×10^{-5} Pa). The thickness of the active layer was measured using an AlphaStep® IQ surface profiler (KLA Tencor).

The current density–voltage ($J-V$) characteristics were measured in the dark under a nitrogen atmosphere using a Keithley 2401 semiconductor analyzer. Voltage sweeps were performed in the range of 0–6 V, and hole mobility was estimated by fitting a J–V curve using the space charge limited current (SCLC) Equation $J = (9/8)\varepsilon_0\varepsilon_r\mu(V^2/L^3)$, where ε_0 is the permittivity of free space, ε_r is the dielectric constant of the polymer, μ is the hole and electron mobility, L is the thickness of the active layer, and V is the voltage drop across the device ($V = V_{appl} - V_{bi}$), where V_{appl} and V_{bi} are the applied and offset voltages, respectively.

Results and discussion

Synthesis of FOBTzE monomers and its copolymer PFOE4T

The synthetic route of FOBTzE monomer **5** and its copolymer **PFOE4T** are depicted in Scheme 1. FBTzE **1** was synthesized from readily available 4-bromo-5,6-difluorobenzo[*c*][1,2,5]thiadiazole according to our previously reported study [38]. Treatment of FBTzE **1** with *n*-decanol and sodium hydride (NaH) afforded decyloxy-substituted FOBTzE **2** in 94% yield [50]. FOBTzE monomer **5** was then synthesized by dehydrogenative coupling of **2** with 2-bromo-3-(2-hexyldecyl)thiophene (**3**) (Table S1) [38]. When 3-cyclohexyl-2,2-dimethylpropanoic acid (**4**) [46, 51] was used as an additive in the dehydrogenative coupling of **2** and **3**, FOBTzE monomer **5** was obtained in 20% isolated yield. Finally, palladium-catalyzed Migita–Kosugi–Stille coupling of FOBTzE monomer **5** and 5,5'-bis(trimethylstannyl)-2,2'-bithiophene (**6**) gave the target copolymer **PFOE4T** in 88% yield as a chlorobenzene fraction. In the case of the previously reported **PFE4T**, the GPC curve exhibited distinct dual peaks, a very high number-average molecular weight (M_n = 133.8 kDa), and a relatively large polydispersity index (PDI = 2.39) due to its strong aggregation tendency [38]. On the other hand, **PFOE4T** showed a single broad GPC curve (Fig. S2), with a standard PDI of 2.04 and a high M_n value of 54.3 kDa. The solubility of **PFOE4T** in chlorobenzene at 80 °C was 4.0 mg/mL, which was higher than that of **PFE4T** (1.5 mg/mL). These results indicate that the introduction of an alkoxy side chain instead of a fluorine atom in the core of FBTzE can reduce the excessively strong aggregation behavior of the polymers.

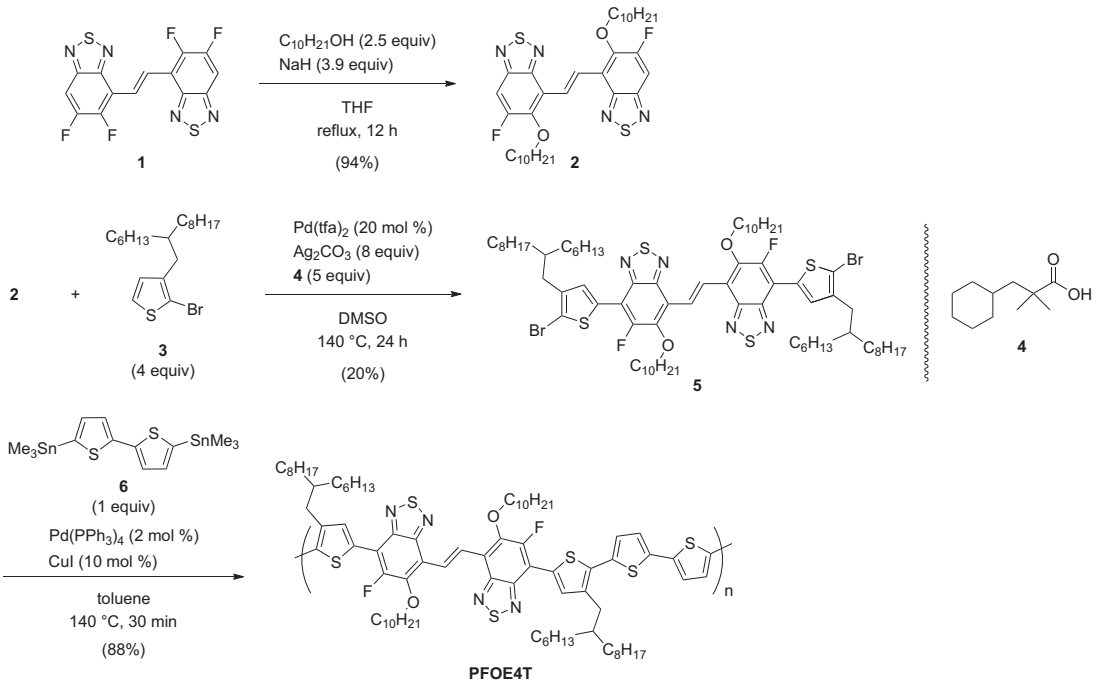

Scheme 1 Synthetic route of FOBTzE monomer **5** and its copolymer **PFOE4T**

Physicochemical properties of FOBTzE-based polymer PFOE4T

Differential scanning calorimetry (DSC) curves of **PFOE4T** and **PFE4T** are depicted in Fig. S3 to investigate the thermal stability of the polymers. No obvious thermal transitions were observed for either **PFOE4T** or **PFE4T** at temperatures of 25–250 °C. This indicates that **PFOE4T** is a thermodynamically stable polymer even in the solid state, despite its flexible alkoxy chains.

Figure 2a shows the UV–vis absorption spectra of the chlorobenzene solution and thin films of **PFOE4T**, and the extracted data are summarized in Table 1. In solution at room temperature, **PFOE4T** exhibited a single broad absorption with an absorption maximum (λ_{max}) of 610 nm and a weak shoulder peak at 705 nm. When the solution of **PFOE4T** was heated ca. 80 °C, a 40 nm blueshift was observed, and the shoulder peak disappeared completely. This indicates that **PFOE4T** is easily disaggregated by heating ca. 80 °C, and that intermolecular interaction is weaker than that of **PFE4T** [38], which is consistent with the GPC results. In the thin film, a 20 nm redshifted absorption and a more intense shoulder peak at 705 nm were observed, implying the formation of well-ordered packing structures in the solid state. The optical energy gap (E_g^{opt}) was found to be 1.60 eV, which is similar to that of **PFE4T** ($E_g^{opt} = 1.55$ eV) [38].

A cyclic voltammogram of **PFOE4T** in thin films was performed to estimate its frontier orbital energy (Fig. 2b). The estimated HOMO and LUMO energy levels are also summarized in Table 1. The estimated HOMO (E_{HOMO}) and LUMO (E_{LUMO}) energy levels of **PFOE4T** are −5.23 and −3.54 eV, respectively, which are ca. 0.1 eV higher than **PFE4T**. This may be attributed to the introduction of a strong electron-donating alkoxy group into the core of FBTzE instead of an electron-withdrawing fluorine atom. However, the HOMO energy level of **FOE4T** is comparable to that of the 5,6-difluorobenzothiadiazole-based polymer **PffBT4T-DT** [38].

Theoretical calculations of FOBTzE-based copolymer PFOE4T

To understand the electronic structure in detail, DFT calculations for the model compound of **PFOE4T** were carried out (Fig. S1). Here, the methyl group was used as the solubilizing group to simplify the calculations. The calculated HOMO and LUMO coefficients of **PFOE4T** were found to be strongly located at the 5,6-position of the 5-alkoxy-6-fluorobenzo[*c*][1,2,5]thiadiazole moiety. Therefore, the calculated HOMO and LUMO energy levels of **PFOE4T** (HOMO = − 5.20 eV, LUMO = − 3.04 eV) are ca. 0.2 eV higher than those of the model compound of **PFE4T** (HOMO = − 5.36 eV, LUMO = − 3.22 eV) due to the introduction of a strong electron-donating alkoxy group instead of the electron-withdrawing fluorine atom, which is consistent with the results of the CV measurements. TD-DFT calculations for the model

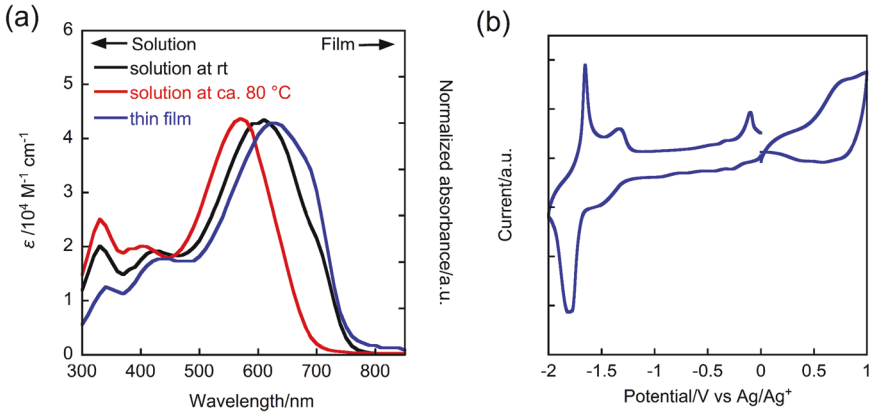

Fig. 2 **a** UV–vis absorption spectra and **b** cyclic voltammogram of **PFOE4T**

Table 1 Physicochemical properties of **PFOE4T**

Polymer	$\lambda_{max,sol}$/nm[a]	$\lambda_{max,film}$/nm[b]	E_g^{opt} (E_g^{CV})/eV[c]	E_{HOMO}/eV[d]	E_{LUMO}/eV[e]
PFOE4T	610	630	1.60 (1.69)	−5.23	−3.54
PFE4T[f]	643, 704	636, 698	1.55 (1.64)	−5.33	−3.69

[a]Absorption maxima in chlorobenzene solution at rt

[b]Absorption maxima in thin film

[c]Optical energy gaps estimated from the absorption edge (λ_{edge}) (out of parentheses) and electrochemical gap (in parentheses)

[d]All the potentials were calibrated with the standard ferrocene/ferrocenium redox couple (Fc/Fc^+: $E^{1/2} = +0.03$ V measured under identical conditions). Estimated with the oxidation onset vs. Ag/Ag^+; $E_{HOMO} = -4.77 - E^{ox}_{onset}$

[e]Estimated with the reduction onset vs. Ag/Ag^+; $E_{LUMO} = -4.77 - E^{red}_{onset}$

[f]Ref. [38]

compounds were performed to confirm the transitions in UV–vis absorption of **PFOE4T** and **PFE4T** (Fig. S1 and Table S2). The excitation wavelengths of the first excitation of **PFOE4T** and **PFE4T** were 653.51 nm and 653.62 nm, respectively. These first excitations originate from the HOMO → LUMO transition of **PFOE4T** and **PFE4T**. These calculated results are in good agreement with the actual UV–vis absorption spectra of the respective polymers.

Figure 3 shows the optimized molecular geometry of the dimeric structure of **PFOE4T** calculated by using M06-2X/6-311 G(d). The N-H, O-H, and F-S distances of the central FOBTzE framework and the neighboring thiophene units are 2.27-2.28 Å, 2.36 Å, and 2.71 Å, respectively, which are significantly smaller than the sum of van der Waals radii (N-H: 2.75 Å, O-H: 2.50 Å, and F-S: 3.17 Å) [45, 52, 53]. Thus, the dihedral angles of the vinylene moiety at the central BTz (φ_1) and the thiophene ring adjacent to BTz (φ_2) are 7.4° and 2.7°, respectively, due to the contribution of intramolecular noncovalent interactions. Because of these multiple conformational locks, **PFOE4T** has a rigid and highly coplanar structure even when an alkoxy side chain is introduced instead of the fluorine atom, resulting in the strong aggregation tendency of **PFOE4T**.

Photovoltaic properties of PFOE4T-based OPVs

To evaluate the potential of **PFOE4T** for OPVs, typical inverted solar cells with a device architecture of ITO/ZnO/**PFOE4T**:$PC_{61}BM$/MoO_3 (6 nm)/Ag (50 nm) were fabricated and characterized. The best current density (*J*)-voltage (*V*) curve under AM 1.5 G simulated solar irradiation of 100 mW cm^{-2} is shown in Fig. 4, and the extracted solar cell parameters are summarized in Table S3. [6,6]-Phenyl-C_{61}-butyric acid methyl ester ($PC_{61}BM$) was used as the n-type material. The best ratio of polymer to $PC_{61}BM$ (p/n ratio) is 1:1. Since **PFOE4T** has weaker aggregation than **PFE4T**, a uniform thin film could be obtained. Optimization of the spin-coating solvent and additives resulted in the best solar cell performance when chlorobenzene with 1 vol% diphenyl ether (DPE) was used. The **PFOE4T**-based solar cell exhibited a V_{oc} of 0.74 V, which was 0.06 V lower value than the previously reported FBTzE-thienothiophene copolymer-based solar cell [38] due to the upshifted HOMO energy level of **PFOE4T** [8, 9]. As a result, the **PFOE4T**-based solar cell exhibited a PCE of 4.52% at J_{sc} of 9.04 mA cm^{-2} and a high FF of 0.68. To further understand the solar cell performance of **PFOE4T**, a hole-only

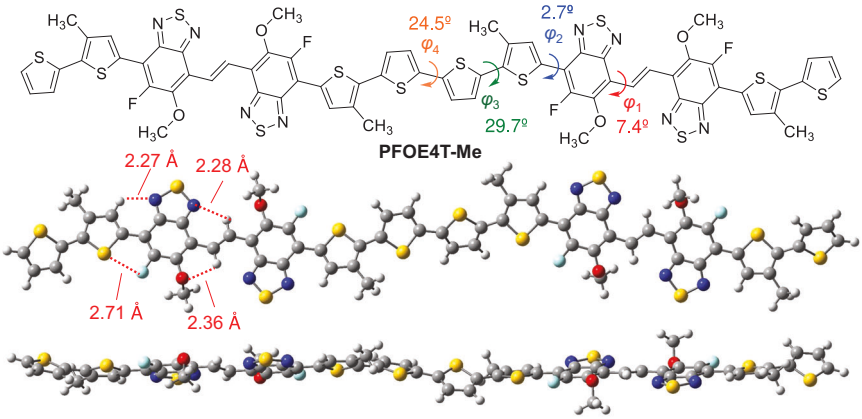

Fig. 3 Optimized molecular geometry of the dimeric structure of **PFOE4T** by DFT calculations (M06-2X/6-311 G(d))

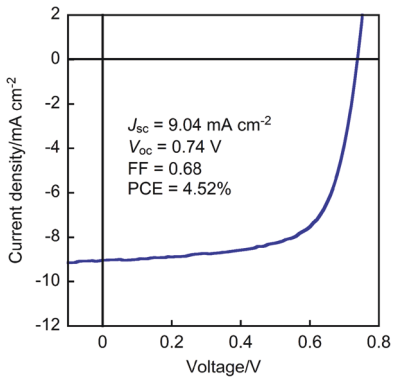

Fig. 4 *J*–*V* curve of the best **PFOE4T**/$PC_{61}BM$-based solar cell

device with an ITO/(PEDOT:PSS)/**PFOE4T**:$PC_{61}BM$/MoO_3 (6 nm)/Ag (100 nm) structure and an electron-only device with an ITO/ZnO/**PFOE4T**:$PC_{61}BM$/Ag (100 nm) structure were fabricated and evaluated to estimate the hole and electron mobility using the SCLC method (Fig. S4). The estimated SCLC hole ($\mu_{SCLC,h}$) and electron ($\mu_{SCLC,e}$) mobilities were 4.69×10^{-4} cm^2 V^{-1} s^{-1} and 2.57×10^{-4} cm^2 V^{-1} s^{-1}, respectively, with a mobility balance (μ_h/μ_e) of 1.82. Such a good mobility balance effectively prevents bimolecular recombination losses, which would lead to a high FF of 0.68 [54].

Morphological study of PFOE4T/$PC_{61}BM$ blended films by GIWAXS and AFM analysis

To evaluate the relationship between the thin-film structure and photovoltaic properties, grazing incidence wide-angle X-ray scattering (GIWAXS) measurements were performed (Figs. 5a, b and S5). In pure **PFOE4T** films, (100) and (010) diffractions were observed in both the q_z and q_{xy} axes, assigned to lamellar and π-stacking structures of the polymer (Fig. 5a). These diffractions indicate that neat **PFOE4T** formed a bimodal orientation with a lamellar distance (d_{lm}) of 19.7 Å and a π-stacking distance (d_π) of 3.83 Å. In addition, ring-shaped (100) and (010) diffractions were also observed in the **PFOE4T**/$PC_{61}BM$ blended film (Fig. 5b), indicating that **PFOE4T** formed a randomly oriented structure in the blended film. In comparison to **PFE4T**, **PFOE4T** has a better molecular orientation for carrier transport in OPVs [14] since **PFE4T** forms an unfavorable edge-on orientation [39]. One possible reason for the change in molecular orientation of **PFOE4T** could be an increase in the attachment density of the side chains, which may have suppressed the construction of interdigitated lamellar structures [14, 18, 55]. Thus, the **PFOE4T**/$PC_{61}BM$ blended film showed high hole mobility, resulting in high FF. We also demonstrated that the introduction of alkoxy groups instead of fluorine atoms in the FBTzE core can control the molecular orientation as well as solubility of the polymer.

Figure 5c shows the surface morphology of the **PFOE4T**/$PC_{61}BM$ blended film as measured by atomic force microscopy (AFM). Both the topographic and error-signal images showed that the root–mean–square (RMS) value of the **PFOE4T**/$PC_{61}BM$ blended film is relatively small (RMS = 0.95 nm). However, the **PFOE4T**/$PC_{61}BM$ blended film formed sphere-like large domains, with domain sizes exceeding 100 nm, likely due to the still low solubility and strong aggregation ability of **PFOE4T**. Such a large-scale phase separation structure may strongly inhibit exciton dissociation, leading to a limitation of J_{sc} and hence of PCE [15–17].

Conclusion

In summary, we have successfully synthesized a FOBTzE-quarterthiophene copolymer **PFOE4T** with a vinylene-bridged 5-alkoxy-6-fluorobenzo[*c*][1,2,5]thiadiazole (FOBTzE) core and improved the too strong aggregation behavior and molecular orientation of the previously reported polymer **PFE4T** based on vinylene-bridged 5,6-difluorobenzo[*c*][1,2,5]thiadiazole (FBTzE). Although the installation of an alkoxy group instead of a fluorine atom in the FBTzE core led to elevation of

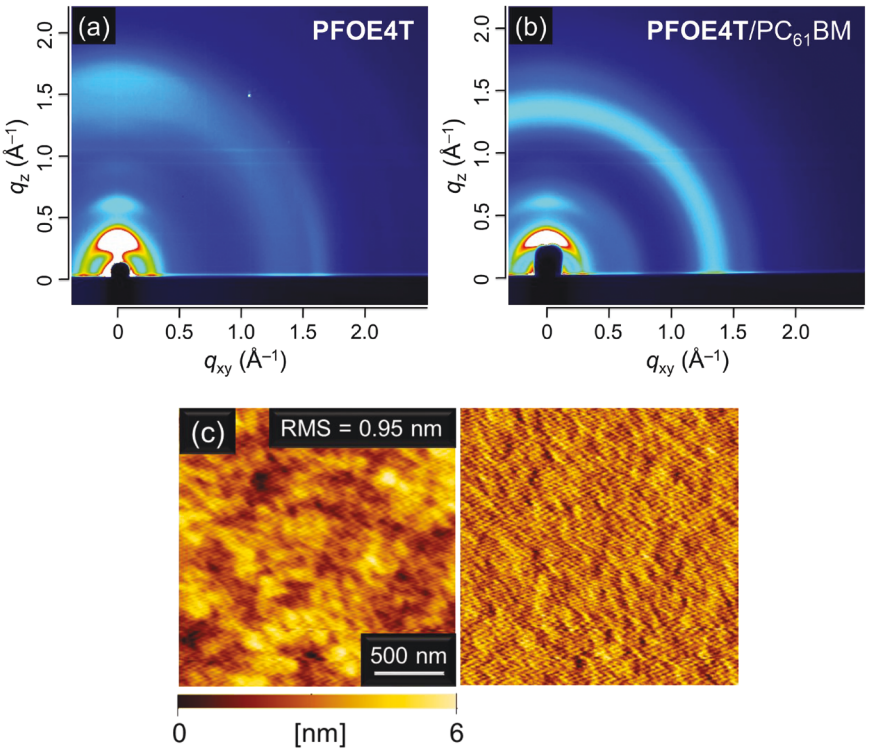

Fig. 5 GIWAXS images of **PFOE4T** films on ZnO-treated ITO substrate; **a** neat **PFOE4T** film and **b** **PFOE4T**/$PC_{61}BM$ blended film. **c** Topographic (left) and error-signal (right) images of **PFOE4T** film blended with $PC_{61}BM$ on ZnO-treated ITO substrate

the HOMO energy level of the resulting polymer, the aggregation ability of **PFOE4T** was reduced, resulting in a uniform thin film of **PFOE4T** blended with $PC_{61}BM$. Furthermore, the presence of additional alkoxy side chains in the FOBTzE core can change the molecular orientation of the polymer from edge-on to bimodal. As a result, the **PFOE4T**/$PC_{61}BM$-based solar cell exhibited high hole mobility and good mobility balance, leading to high FF. However, the low solubility and strong aggregation tendency of **PFOE4T** may promote large-scale phase separation in the blended film with $PC_{61}BM$, preventing efficient photocurrent conversion, resulting in a limited J_{sc} and thus a PCE of 4.52%. However, the morphology and electronic structure can be easily controlled by optimizing the choice of side chains and donor units. Thus, the FOBTzE core may be a potential building block for high-performance D-A-type π-conjugated polymers in OPVs.

Acknowledgements This study was supported in part by Grant-in-Aid for Young Scientists (No. 19K15650) from the Japan Society for the Promotion of Science, Okayama Prefecture Industrial Promotion Foundation, and the Yakumo Foundation for Environmental Science. The GIWAXS experiments were performed at BL13XU and BL46XU of SPring-8 with the approval of the Japan Synchrotron Radiation Research Institute (JASRI) (Proposals 2019A1765 and 2022A1656). We are grateful to Prof. Itaru Osaka, and Dr. Masahiko Saito (Hiroshima University), as well as Dr. Tomoyuki Koganezawa (JASRI), for measurements of GIWAXS images; Prof. Koichi Mitsudo and Prof. Seiji Suga (Okayama University) for CV measurements; Prof. Tsutomu Ono and Prof. Takaichi Watanabe (Okayama University) for DSC measurements; Prof. Naoshi Ikeda (Okayama University) for AFM images; Prof. Yoshihiro Kubozono (Okayama University) for thickness measurements; and Megumi Kosaka and Motonari Kobayashi at the Department of Instrumental Analysis, Advanced Science Research Center, Okayama University, for elemental analysis measurements. We also thank the SC-NMR Laboratory of Okayama University for the NMR spectral measurements.

Compliance with ethical standards

Conflict of interest The authors declare no competing interests.

References

1. Cheng Y-J, Yang S-H, Hsu C-S. Synthesis of conjugated polymers for organic solar cell applications. Chem Rev. 2009;109:5868–923.
2. Zhou H, Yang L, You W. Rational design of high performance conjugated polymers for organic solar cells. Macromolecules. 2012;45:607–32.
3. Lu L, Zheng T, Wu Q, Schneider AM, Zhao D, Yu L. Recent advances in bulk heterojunction polymer solar cells. Chem Rev. 2015;115:12666–731.
4. Cai Y, Huo L, Sun Y. Recent advances in wide-bandgap photovoltaic polymers. Adv Mater. 2017;29:1605437.
5. Cui C, Li Y. High-performance conjugated polymer donor materials for polymer solar cells with narrow-bandgap nonfullerene acceptors. Energy Environ Sci. 2019;12:3225–46.
6. Mori H, Nishihara Y. Low-bandgap semiconducting polymers based on sulfur-containing phenacene-type molecules for transistor and solar cell applications. Polym J. 2018;50:615–25.
7. Saito M, Ohkita H, Osaka I. π-Conjugated polymers and molecules enabling small photon energy loss simultaneously with high efficiency in organic photovoltaics. J Mater Chem A. 2020;8:20213–37.
8. Scharber MC, Mühlbacher D, Koppe M, Denk P, Waldauf C, Heeger AJ, et al. Design rules for donors in bulk-heterojunction solar cells—towards 10% energy-conversion efficiency. Adv Mater. 2006;18:789–94.

9. Dennler G, Scharber MC, Brabec CJ. Polymer-fullerene bulk-heterojunction solar cells. Adv Mater. 2009;21:1323–38.
10. Yao J, Kirchartz T, Vezie MS, Faist MA, Gong W, He Z, et al. Quantifying losses in open-circuit voltage in solution-processable solar cells. Phys Rev Appl. 2015;4:014020.
11. Menke SM, Ran NA, Bazan GC, Friend RH. Understanding energy loss in organic solar cells: toward a new efficiency regime. Joule. 2018;2:25–35.
12. Zhang G, Zhao J, Chow PCY, Jiang K, Zhang J, Zhu Z, et al. Nonfullerene acceptor molecules for bulk heterojunction organic solar cells. Chem Rev. 2018;118:3447–507.
13. Fu H, Wang Z, Sun Y. Polymer donors for high-performance non-fullerene organic solar cells. Angew Chem Int Ed. 2019;58:4442–53.
14. Osaka I, Takimiya K. Backbone orientation in semiconducting polymers. Polymer. 2015;59:A1–A15.
15. Huang Y, Kramer EJ, Heeger AJ, Bazan GC. Bulk heterojunction solar cells: morphology and performance relationships. Chem Rev. 2014;114:7006–43.
16. Ye L, Collins BA, Jiao X, Zhao J, Yan H, Ade H. Miscibility-function relations in organic solar cells: significance of optimal miscibility in relation to percolation. Adv Energy Mater. 2018;8:1703058.
17. Lee H, Park C, Sin DH, Park JH, Cho K. Recent advances in morphology optimization for organic photovoltaics. Adv Mater. 2018;30:1800453.
18. Mori H, Takahashi R, Hyodo K, Nishinaga S, Sawanaka Y, Nishihara Y. Phenanthrodithiophene (PDT)−difluorobenzothiadiazole (DFBT) copolymers: Effect on molecular orientation and solar cell performance of alkyl substitution onto a PDT core. Macromolecules. 2018;51:1357–69.
19. Wang Y, Michinobu T. Benzothiadiazole and its π-extended, heteroannulated derivatives: useful acceptor building blocks for high-performance donor-acceptor polymers in organic electronics. J Mater Chem C. 2016;4:6200–14.
20. Wang C, Liu F, Chen Q-M, Xiao C-Y, Wu Y-G, Li W-W. Benzothiadiazole-based conjugated polymers for organic solar cells. Chin J Polym Sci. 2021;39:525–36.
21. Lee W, Kim G-H, Ko S-J, Yum S, Hwang S, Cho S, et al. Semi-crystalline D−A copolymers with different chain curvature for applications in polymer optoelectronic devices. Macromolecules. 2014;47:1604–12.
22. Kini GP, Oh S, Abbas Z, Rasool S, Jahandar M, Song CE, et al. Effects on photovoltaic performance of dialkyloxy-benzothiadiazole copolymers by varying the thienoacene donor. ACS Appl Mater Interfaces. 2017;9:12617–28.
23. Ko S-J, Hoang QV, Song CE, Uddin MA, Lim E, Park SY, et al. High-efficiency photovoltaic cells with wide optical band gap polymers based on fluorinated phenylene-alkoxybenzothiadiazole. Energy Environ Sci. 2017;10:1443–55.
24. Lin Y, Zhao F, Wu Y, Chen K, Xia Y, Li G, et al. Mapping polymer donors toward high-efficiency fullerene free organic solar cells. Adv Mater. 2017;29:1604155.
25. Casey A, Ashraf RS, Fei Z, Heeney M. Thioalkyl-substituted benzothiadiazole acceptors: copolymerization with carbazole affords polymers with large stokes shifts and high solar cell voltages. Macromolecules. 2014;47:2279–88.
26. Chen Z, Cai P, Chen J, Liu X, Zhang L, Lan L, et al. Low band-gap conjugated polymers with strong interchain aggregation and very high hole mobility towards highly efficient thick-film polymer solar cells. Adv Mater. 2014;26:2586–91.
27. Liu Y, Zhao J, Li Z, Mu C, Ma W, Hu H, et al. Aggregation and morphology control enables multiple cases of high-efficiency polymer solar cells. Nat Commun. 2014;5:5293.
28. Zhao J, Li Y, Yang G, Jiang K, Lin H, Ade H, et al. Efficient organic solar cells processed from hydrocarbon solvents. Nat Energy. 2016;1:15027.
29. Mori H, Nonobe H, Nishihara Y. Highly crystalline, low band-gap semiconducting polymers based on phenanthrodithiophene-benzothiadiazole for solar cells and transistors. Polym Chem. 2016;7:1549–58.
30. Feng L-W, Chen J, Mukherjee S, Sangwan VK, Huang W, Chen Y, et al. Readily accessible benzo[*d*]thiazole polymers for non-fullerene solar cells with >16% efficiency and potential pitfalls. ACS Energy Lett. 2020;5:1780–7.
31. Hu Z, Chen H, Qu J, Zhong X, Chao P, Xie M, et al. Design and synthesis of chlorinated benzothiadiazole-based polymers for efficient solar energy conversion. ACS Energy Lett. 2017;2:753–8.
32. Yang Z, Chen H, Wang H, Mo D, Liu L, Chao P, et al. The integrated adjustment of chlorine substitution and two-dimensional side chain of low band gap polymers in organic solar cells. Polym Chem. 2018;9:940–7.
33. Olla T, Ibraikulov OA, Ferry S, Boyron O, Méry S, Heinrich B, et al. Benzothiadiazole halogenation impact in conjugated polymers, a comprehensive study. Macromolecules. 2019;52:8006–16.
34. Kini GP, Choi JY, Jeon SJ, Suh IS, Moon DK. Effect of mono alkoxy-carboxylate-functionalized benzothiadiazole-based donor polymers for non-fullerene solar cells. Dyes Pigments. 2019;164:62–71.
35. Casey A, Han Y, Fei Z, White AJP, Anthopoulos TD, Heeney M. Cyano substituted benzothiadiazole: a novel acceptor inducing n-type behaviour in conjugated polymers. J Mater Chem C. 2015;3:265–75.
36. Shi S, Chen P, Chen Y, Feng K, Liu B, Chen J, et al. A narrow-bandgap n-type polymer semiconductor enabling efficient all-polymer solar cells. Adv Mater. 2019;31:1905161.
37. Li G, Kang C, Gong X, Zhang J, Li C, Chen Y, et al. 5-Alkyloxy-6-fluorobenzo[*c*][1,2,5]thiadiazole- and silafluorene-based D−A alternating conjugated polymers: synthesis and application in polymer photovoltaic cells. Macromolecules. 2014;47:4645–52.
38. Asanuma Y, Mori H, Takahashi R, Nishihara Y. Vinylene-bridged difluorobenzo[*c*][1,2,5]thiadiazole (FBTzE): a new electron-deficient building block for high-performance semiconducting polymers in organic electronics. J Mater Chem C. 2019;7:905–16.
39. Asanuma Y, Mori H, Nishihara Y. Transistor properties of semiconducting polymers based on vinylene-bridged difluorobenzo[*c*][1,2,5]thiadiazole (FBTzE). Chem Lett. 2019;48:1029–31.
40. Mori H. Development of semiconducting polymers based on a novel heteropolycyclic aromatic framework. Polym J. 2021;53:975–87.
41. Zhang J, Zhang X, Li G, Xiao H, Li W, Xie S, et al. A non-fullerene acceptor for wide band gap polymer based organic solar cells. Chem Commun. 2016;52:469–72.
42. Li G, Zhao B, Kang C, Lu Z, Li C, Dong H, et al. Side chain influence on the morphology and photovoltaic performance of 5-fluoro-6-alkyloxybenzothiadiazole and benzodithiophene based conjugated polymers. ACS Appl Mater Interfaces. 2015;7:10710–7.
43. Zhou Y, Li M, Guo Y, Lu H, Song J, Bo Z, et al. Dibenzopyran-based wide band gap conjugated copolymers: structural design and application for polymer solar cells. ACS Appl Mater Interfaces. 2016;8:31348–58.
44. Gong X, Li G, Wu Y, Zhang J, Feng S, Liu Y, et al. Enhancing the performance of polymer solar cells by using donor polymers carrying discretely distributed side chains. ACS Appl Mater Interfaces. 2017;9:24020–6.
45. Huang H, Yang L, Facchetti A, Marks TJ. Organic and polymeric semiconductors enhanced by noncovalent conformational locks. Chem Rev. 2017;117:10291–318.
46. Fujihara T, Yoshida A, Satou M, Tanji Y, Terao J, Tsuji Y. Steric effect of carboxylic acid ligands on Pd-catalyzed C–H activation reactions. Catal Commun. 2016;84:71–4.
47. Mori H, Nishinaga S, Takahashi R, Nishihara Y. Alkoxy-substituted anthra[1,2-*c*:5,6-*c*']bis([1,2,5]thiadiazole) (ATz): A

new electron-acceptor unit in the semiconducting polymers for organic electronics. Macromolecules. 2018;51:5473–84.
48. Frisch MJ, Trucks GW, Schlegel HB, Scuseria GE, Robb MA, Cheeseman JR, et al. *Gaussian 09, Revision D.01*. Wallingford, CT: Gaussian, Inc.; 2013.
49. Mori H, Hara S, Nishinaga S, Nishihara Y. Solar cell performance of phenanthrodithiophene−isoindigo copolymers depends on their thin-film structure and molecular weight. Macromolecules. 2017; 50:4639–48.
50. Kini GP, Lee SK, Shin WS, Moon S-J, Song CE, Lee J-C. Achieving a solar power conversion efficiency exceeding 9% by modifying the structure of a simple, inexpensive and highly scalable polymer. J Mater Chem A. 2016;4:18585–97.
51. Tanji Y, Mitsutake N, Fujihara T, Tsuji Y. Steric effect of carboxylate ligands on Pd-catalyzed intramolecular $C(sp^2)$–H and $C(sp^3)$–H arylation reactions. Angew Chem Int Ed. 2018;57:10314–7.
52. Wen T-J, Liu Z-X, Chen Z, Zhou J, Shen Z, Xiao Y, et al. Simple non-fused electron acceptors leading to efficient organic photovoltaics. Angew Chem Int Ed. 2021;60:12964–70.
53. Bondi A. van der Waals volumes and radii. J Phys Chem. 1964; 68:441–51.
54. Tress W, Petrich A, Hummert M, Hein M, Leo K, Riede M. Imbalanced mobilities causing S-shaped IV curves in planar heterojunction organic solar cells. Appl Phys Lett. 2011;98: 063301.
55. Zhang X, Richter LJ, DeLongchamp DM, Kline RJ, Hammond MR, McCulloch I, et al. Molecular packing of high-mobility diketopyrrolo-pyrrole polymer semiconductors with branched alkyl side chains. J Am Chem Soc. 2011;133:15073–84.